# Vascularized pulp regeneration via injecting simvastatin functionalized GelMA cryogel microspheres loaded with stem cells from human exfoliated deciduous teeth

Xiaojing Yuan [a,1], Zuoying Yuan [b,1], Yuanyuan Wang [a], Zhuo Wan [c], Xiaotong Wang [d], Shi Yu [a], Jianmin Han [e], Jianyong Huang [b], Chunyang Xiong [b,f,*], Lihong Ge [a,**], Qing Cai [c], Yuming Zhao [a,***]

[a] Department of Pediatric Dentistry, Peking University School and Hospital of Stomatology & National Center of Stomatology & National Clinical Research Center for Oral Diseases & National Engineering Laboratory for Digital and Material Technology of Stomatology & Beijing Key Laboratory of Digital Stomatology, No.22, Zhongguancun South Avenue, Haidian District, Beijing, 100081, PR China
[b] Department of Mechanics and Engineering Science, College of Engineering, Peking University, Beijing, 100871, China
[c] State Key Laboratory of Organic-Inorganic Composites; Beijing Laboratory of Biomedical Materials; Beijing University of Chemical Technology, Beijing, 100029, China
[d] Department of Emergency, Peking University School and Hospital of Stomatology & National Center of Stomatology & National Clinical Research Center for Oral Diseases & National Engineering Laboratory for Digital and Material Technology of Stomatology, No.22, Zhongguancun South Avenue, Haidian District, Beijing, 100081, PR China
[e] Dental Medical Devices Testing Center, Dental Materials Laboratory, Peking University School and Hospital of Stomatology & National Center of Stomatology & National Clinical Research Center for Oral Diseases & National Engineering Laboratory for Digital and Material Technology of Stomatology, No.22, Zhongguancun South Avenue, Haidian District, Beijing, 100081, PR China
[f] Academy for Advanced Interdisciplinary Studies, Peking University, Beijing, 100871, China

## ARTICLE INFO

## ABSTRACT

Dental pulp necrosis are serious pathologic entities that causes tooth nutrition deficiency and abnormal root development, while regeneration of functional pulp tissue is of paramount importance to regain tooth vitality. However, existing clinical treatments, which focus on replacing the necrotic pulp tissue with inactive filling materials, fail to restore pulp vitality and functions, thus resulting in a devitalized and weakened tooth. Currently, dental pulp regeneration via stem cell-based therapy for pulpless teeth has raised enormous attention to restore the functional pulp. Here, a novel design of injectable simvastatin (SIM) functionalized gelatin methacrylate (GelMA) cryogel microspheres (SMS) loaded with stem cells from human exfoliated deciduous teeth (SHEDs) was established to refine SHEDs biological behaviors and promote *in vivo* vascularized pulp-like tissue regeneration. In this system, SIM encapsulated poly (lactide-*co*-glycolide) (PLGA) nanoparticles were incorporated into GelMA cryogel microspheres via cryogelation and $O_1/W/O_2$ emulsion method. SMS with sustained release of SIM promoted SHEDs adhesion, proliferation and exhibited cell protection properties during the injection process. Furthermore, SMS enhanced SHEDs odontogenic differentiation and angiogenic potential, and SHEDs loaded SMS (SHEDs/SMS) are beneficial for human umbilical vein endothelial cells (HUVECs) migration and angiogenesis, demonstrating their potential for use in promoting vascularized tissue regeneration. SHEDs/SMS complexes were injected into cleaned human tooth root segments for subcutaneous implantation in nude mice. Our results demonstrated that SHEDs/SMS could induce vessel-rich pulp-like tissue regeneration *in vivo* and that such an injectable nano-in-micro multistage system for the controlled delivery of bioactive reagents would be suitable for clinical application in endodontic regenerative dentistry.

---

\* Corresponding author. Department of Mechanics and Engineering Science, College of Engineering, Peking University, Beijing, 100871, China.
\*\* Corresponding author. Department of Pediatric Dentistry, Peking University School and Hospital of Stomatology & National Center of Stomatology & National Clinical Research Center for Oral Diseases & National Engineering Laboratory for Digital and Material Technology of Stomatology & Beijing Key Laboratory of Digital Stomatology, No.22, Zhongguancun South Avenue, Haidian District, Beijing, 100081, PR China.
\*\*\* Corresponding author. Department of Pediatric Dentistry, Peking University School and Hospital of Stomatology & National Center of Stomatology & National Clinical Research Center for Oral Diseases & National Engineering Laboratory for Digital and Material Technology of Stomatology & Beijing Key Laboratory of Digital Stomatology, No.22, Zhongguancun South Avenue, Haidian District, Beijing, 100081, PR China.
*E-mail addresses:* fatulousfie@126.com (X. Yuan), cyxiong@pku.edu.cn (C. Xiong), gelihong0919@163.com (L. Ge), yumingzhao70@sina.com (Y. Zhao).
[1] These two authors contribute equally.

| Abbreviation despcription | | | |
|---|---|---|---|
| SIM | Simavastatin | DMP-1 | Dentin matrix protein-1 |
| GelMA | Gelatin methacrylate | DSPP | Dentin sialophosphoprotein |
| CMS | Cryogel microspheres | VEGF | Vascular endothelial growth factor |
| SMS | SIM functionalized cryogel microspheres | VEGF-R2 | Vascular endothelial growth factor receptor-2 |
| SHEDs | Stem cells from human exfoliated deciduous teeth | SDF-1 | Stromal cell-derived factor-1 |
| PLGA | Poly(lactide-*co*-glycolide) | CXCR-4 | C-X-C chemokine receptor type-4 |
| HUVECs | Human umbilical vein endothelial cells | ALP | Alkaline phosphatase |
| DPSCs | Dental pulp stem cells | HMS | Hydrogel microspheres |
| PM | Proliferation medium | TCPs | Tissue culture plates |
| OM | Odontogenic induced medium | GFP | Green fluorescent protein |
| | | PCS | Post-injection survival |
| | | CAM | Chorioallantoic membrane |

## 1. Introduction

Dental pulp, a soft tissue responsible for tooth nutritional supply, dentin production, and tooth sensation, is crucial for tooth vitality maintenance [1]. However, dental pulp is vulnerable to insults rendered from caries, trauma or idiopathic factors, which are further prone to induce pulp inflammation and even irreversible pulp necrosis [2,3]. Conventional clinical treatments, known as apexification, pulp revascularization, and root canal therapy, are mainly focused on inflammation control by removing necrotic pulp tissue and fill the canals with synthetic biomaterials, while few vital pulp-like tissue is regenerated during the treatment process [4]. Devitalized young permanent teeth inevitably lose the natural biological defence that is inherent in dental pulp and leaves the tooth with thin root canal walls. These weakened teeth are brittle and prone to fracture over time, which seriously affects tooth survival rate [5]. The implications of conventional endodontic treatments have driven extensive interest in facilitating the regeneration of vital pulp tissue. Dental derived stem cells with odontogenic differentiation capacity exhibit potential to regenerate dentin and pulp tissue, and dental stem cells mediated pulp regeneration strategies are increasingly being explored as alternative strategies for restoring devitalized tooth vitality [6,7].

Dental pulp stem cells (DPSCs) have been demonstrated as seeding cells in stem cell-based endodontic regenerative therapy [8,9]. The implantation of DPSCs could promote the regeneration of dental pulp tissue with physiological pulp structure [10], however, DPSCs are usually obtained from adult patients with the requirement of extracting impacted molars. The long tooth extraction process delayed timely stem cell isolation, thus resulting in a confined DPSCs source. Stem cells from human exfoliated deciduous teeth (SHEDs) are harvested from exfoliated deciduous teeth in a minimally invasive way, and exhibit non-immunogenicity and higher proliferative potential than DPSCs [11–13]. SHEDs with multipotent differentiation potential could be applied as an alternative seeding cells for pulp tissue engineering [14], nonetheless, the ability of SHEDs in promoting pulp regeneration in the necrotic pulp microenvironment with vascular formation is still limited.

Various growth factors, such as vascular endothelial growth factor, platelet-derived growth factor, and basic fibroblast growth factor, had been explored as biological cues to regulate stem cells fate for pulp regeneration [15–17]. However, besides expensive price, growth factors showed a limited duration of action due to short half-life and potential side effects [18–20]. Hence, a strong trend is to develop a growth factor free system with stem cell fate regulating property for pulp regeneration. Simvastatin (SIM), a small molecule drug used to treat hyperlipidaemia, has been proven to show multiple functions, including anti-inflammatory and anti-oxidative potential, and to promote mineralized tissue deposition [21–23]. In particular, SIM improved endothelial-specific genes and proteins expression in rat bone marrow-derived mesenchymal stem cells [24], and SIM-releasing chitosan scaffold increased the chemotaxis and regenerative potential of dental pulp cells [25]. We hypothesize that SIM could regulate SHEDs differentiation toward an odontoblastic phenotype and enhance angiogenic potential to promote vascularized pulp regeneration.

An obstacle closely related to pulp tissue engineering strategies using dental stem cells is a low cell retention rate. Considering the unique irregular structure of root canals, the injectable scaffold could be suitable to improve cell retention rate and facilitate clinical injection operations. In this study, we designed injectable SIM functionalized gelatin methacrylate (GelMA) cryogel microspheres (SMS) to effectively deliver SHEDs into root canals, and in situ regulate SHEDs biological behavior for regenerating vascularized pulp-like tissue. SIM was encapsulated into poly (lactide-*co*-glycolide) (PLGA) nanoparticles to sustain SIM release [26,27]. The PLGA/SIM nanoparticles were further encapsulated into GelMA cryogel microspheres via the combination of cryogelation and $O_1/W/O_2$ emulsion method. The intrinsic arginine-glycine-aspartic acid (RGD) peptides of gelatin [28–31] and the porous architecture of cryogel microspheres make SMS a biocompatible vehicle for SHEDs adhesion, proliferation and further protect SHEDs from mechanical damage during the injection process. The sustained release of SIM from SMS enhanced SHEDs odontogenic differentiation and angiogenic potential. Finally, SHEDs loaded SMS was subcutaneously injected into nude mice back directly or injected into human tooth root segments, followed by implanting into the dorsal pockets of nude mice to explore the feasibility of using SHEDs loaded SMS in achieving vascularized pulp tissue regeneration.

## 2. Materials and methods

### 2.1. Materials

Gelatin (type A, from porcine skin, ~300 g Bloom) was purchased from Sigma-Aldrich (USA). Methacrylic anhydride and 2-hydroxy-4'-(2-hydroxyethoxy)-2-methylpropiophenone (I2959) were purchased from Aladdin (China). All other reagents and solvents used were of analytical grade and supplied by Beijing Chemical Reagent Co, Ltd. (China).

### 2.2. SHEDs culture

Stem cells from human exfoliated deciduous teeth (SHEDs) were a gift from the Oral Stem Cell Bank (China, Beijing). These cells were characterized by this public institution and stored in liquid nitrogen vapor for long-term cryopreservation [32]. Briefly, SHEDs were thawed and incubated in α-MEM (Gibco, USA) supplemented with 10% fetal bovine serum (FBS, Gibco, USA) and 1% penicillin-streptomycin (100 U/ml and 100 μg/mL, Invitrogen, UK) in an atmosphere containing 5% $CO_2$ at 37 °C. Three to five passages of SHEDs were used in the experiments.

### 2.3. SIM dosage selection

SHEDs were seeded on 96-well plates (Corning, Corning, NY) (5 ×

$10^3$ cells/well) in complete α-MEM (proliferation medium, PM) and incubated for 24 h. They were then cultured in 100 μL α-MEM supplemented with 0 μM, 0.01 μM, 0.1 μM, 1 μM or 10 μM SIM (Sigma-Aldrich) for 1, 3, 5 and 7 days. The culture medium supplemented or not with SIM was replaced every 48 h. Cell Counting Kit-8 (CCK-8) assay was tested for SHEDs viability. The morphological changes of SHEDs were visualized after 7 days culture in PM by light microscopy (TE2000-U, Nikon, Japan).

SHEDs at a density of $5 \times 10^4$ cells/well were dispersed in 12-well plate and cultured in PM (negative control) and odontogenic induced medium (OM, PM supplemented with potassium dihydrogen phosphate, L-ascorbic acid-2-phosphate, glutamine and dexamethasone) supplemented with 0 μM, 0.01 μM, 0.1 μM and 1 μM of SIM for 7 days. ALP activity, calcium deposition, Dentin matrix protein-1 (DMP-1) and Dentin sialophosphoprotein (DSPP) genes expression were analyzed by ALP staining (Alkaline Phosphatase Color Development kit, CWbio, China), Alizarin Red S staining (ARS, Sigma, USA) and real-time polymerase chain reaction (RT-PCR) to evaluate SHEDs odontogenic potential.

The angiogenic potential and chemokines expression of SHEDs were analyzed by RT-PCR. Briefly, SHEDs were cultured in α-MEM supplemented with 0 μM, 0.01 μM, 0.1 μM and 1 μM of SIM for 7 days in 12-well plates ($5 \times 10^4$ cells/well), vascular endothelial growth factor (VEGF), vascular endothelial growth factor receptor-2 (VEGF-R2), stromal cell-derived factor-1 (SDF-1) and C-X-C chemokine receptor type-4 (CXCR-4) genes expression were determined by RT-PCR. Detailed primers information can be found in the Table S1. The scratch test was performed to explore the effect of SIM stimulated SHEDs conditioned medium on human umbilical vein epithelial cells (HUVECs) migratory ability. Briefly, HUVECs monolayers were scratched with a pipette tip along the diameter of the well. Culture medium from SHEDs stimulated with SIM (0 μM, 0.01 μM, 0.1 μM and 1 μM) were centrifuged respectively and the supernatant medium (conditioned medium) of each concentration group was extracted and added to HUVECs. Cells movement into the blank area were monitored after 24 h. The migration distance of HUVECs was calculated by using the Image J software.

### 2.4. Fabrication of CMS and SMS

GelMA, with ~80% acrylate substitution, was synthesized by reacting gelatin with methacrylic anhydride as previously reported [33]. Ten grams of gelatin was dissolved in 100 mL of phosphate buffered saline (PBS) at 50 °C under continuous stirring. 12 mL of methacrylic anhydride was added dropwise to the solution at 50 °C for 4 h, followed by dialysis (cutoff MW 7 kDa) with deionized water for 5 d at 37 °C. Finally, an aqueous solution containing GelMA was lyophilized for further use. CMS with varied pore sizes was fabricated through the emulsion method and gradient cooling procedure as we previously reported [34], GelMA hydrogel microspheres (HMS) were prepared in a similar way, except no gradient cooling and freeze-drying procedure. Detailed information of HMS and CMS fabrication and topological structure can be found in Table S2. The terms CMS-0, CMS-30, and CMS-60 refer to the time (in min) of the −20 °C stage of the cooling process, and thus relate to the final pore diameters. CMS with an optimized pore size was then used for subsequent SMS fabrication.

SMS was fabricated through the combination of the $O_1/W/O_2$ double emulsion method and gradient cooling procedure. Briefly, GelMA (1 g), Tween 60 (20 mg) and I2959 (20 mg) were dissolved in DI water at 40 °C to form a 5% w/v GelMA solution. SIM (0.14 mg), PLGA (0.1 g) and Span 80 (2 mg) were dissolved in 2 mL dichloromethane to form a PLGA/SIM solution. The PLGA/SIM solution was added to GelMA solution and ultrasonicated for 3 min at 200 W in an ice water bath environment to form an $O_1/W$ emulsion. The $O_1/W$ emulsion was then dropwise added into 200 mL of liquid paraffin containing Span 80 (200 mg) with continuous stirring (300 rpm) for 30 min to form an $O_1/W/O_2$ emulsion at room temperature, and the $O_1/W/O_2$ emulsion was then stirred in an ice bath for another 30 min, thereby allowing GelMA to temporarily physically crosslink. Afterwards, the obtained $O_1/W/O_2$ emulsion was

cooled at −20 °C for 30 min and frozen completely in liquid nitrogen. Finally, the chilled emulsion was exposed to 365 nm ultraviolet light to initiate photocrosslinking at an intensity of 40 mW cm$^{-2}$ for 1 min, washed several times with acetone and DI water in sequence, and lyophilized to obtain SMS.

### 2.5. Characterizations of CMS and SMS

The morphology of CMS and SMS was observed by optical microscopy and SEM. The mean diameters (macro axis) of microspheres were calculated by measuring ~100 microspheres from multiple optical microscope photographs while the mean pore sizes (minor axis) of microspheres were measured from multiple SEM photographs using Image J software. PLGA nanoparticles in the GelMA solution were characterized via dynamic light scattering (DLS). For degradation tests, SMS were initially weighed ($W_0$) and then immersed continuously for 12 h in 2 U/mL collagenase solution at 37 °C. At each time point, the collagenase solution was removed from 3 replicates, and they were washed, freeze-dried, and weighed as $W_t$ [35]. The residual mass ratio was determined as:

$$\text{Mass remaining \%} = W_t/W_0 \times 100\%$$

### 2.6. Sustained release of SIM from SMS

The release profile of SIM from the SMS was evaluated in phosphate-buffered saline (PBS) using an elution method. Briefly, 20 mg of SMS were incubated in 10 mL sterile PBS containing 1% antibiotic for pre-determined time points. The supernatants were collected at each time point and replaced with an equal volume of fresh PBS. The released SIM was quantified by a UV–visible spectrophotometer (U-2900 Hitachi) at 238 nm and the amount of released drug was quantified by comparison to the standard curve of SIM [36].

Drug loading rate and encapsulation efficiency were determined as [37]:

Drug Loading Rate= (weight of SIM/weight of SMS) × 100%

Encapsulation Efficiency = drug loading/theoretical drug loading × 100%

### 2.7. Characterizations of cell adhesion and proliferation on CMS and SMS

SHEDs ($5 \times 10^3$ cells/well) were cultured on tissue culture plates (TCPs), CMS (0.2 mg/well) and SMS (0.2 mg/well) with 100 μL α-MEM for 1, 3, 5 and 7 days, and SHEDs proliferation capacity was evaluated by CCK-8 assay. For microsphere-based cell culture, concentrated SHEDs suspension (20 μL) were seeded onto CMS and SMS and co-cultured for 4 h to achieve cell attachment, and then supplementary medium was added [38,39]. After green fluorescent protein (GFP) transduction and antibiotic selection, GFP-labeled cells were cultured in PM for 1 and 7 days for cells distribution observation.

To observe the adhesion morphology of SHEDs on CMS and SMS, SHEDs were cultured in PM for 1 day, SHEDs loaded microspheres were then immediately rinsed with PBS and soaked for 20 min in glutaraldehyde at 4 °C. The fixed samples were dehydrated through a series of ethanol solutions (i.e., 70%, 80%, 90%, and 100%), 2 mL hexamethyldisilazane was added and functioned for 2 min and dried under vacuum. Specimens were coated with platinum-palladium using an auto fine coater (JEOL JEC-3000 FC), and then examined by SEM. For RT-PCR assays, SHEDs were rinsed with PBS after cultured on TCPs, CMS and SMS for 1 day, and TRIzol reagent (Invitrogen, USA) was added to each well to extract total RNA. RNA was reverse-transcribed to cDNA following the manufacturer's instructions (Takara, Japan). RT-PCR was performed using the SYBR Green RT-PCR Kit (Takara, Japan). *GAPDH* served as a housekeeping gene for the normalization of data. The specific

adhesion marker gene primer for integrin-β1 (ITG-β1) was listed in Table S1.

For immunofluorescence staining of phalloidin and vinculin, SHEDs were seeded at the density of $2.5 \times 10^4$ cells per well on 1 mg CMS or SMS, and dispersed in 24-well plates. After 72 h of incubation, SHEDs were washed with PBS, fixed with 4% paraformaldehyde in PBS for 15 min, permeabilized in 0.2% Triton X-100 for 10 min, and then blocked with 1% bovine serum albumin (BSA) for 1 h. The samples were incubated with vinculin primary antibody (1:300, Proteintech, USA) overnight at 4 °C. Secondary fluorescent antibodies were incubated for 1 h. Cytoskeletal fibers were stained with phalloidin (1:200, Yeasen, China) for 20 min and nuclear counterstaining was performed for 10 min at room temperature. Then samples were imaged with a Leica Microsystems CMS GmbH (TCS SP8 X, Germany). To further evaluate the biocompatibility of CMS and SMS and observe SHEDs growth patterns, SHEDs were cultured in PM for 7 days and samples were prepared as aforementioned methods, cytoskeleton was stained with phalloidin and observed by confocal laser scanning microscope (CLSM).

### 2.8. "Post-injection cell survival" (PCS) experiment

The PCS experiment of microspheres was designed according to the previous work [40]. Briefly, SHEDs ($3 \times 10^3$ cells/well) were seeded on microspheres and dispersed in 96-well plates. These microspheres were taken up into a 1 mL syringe with a 26 G needle (inner diameter = 0.25 mm) after 3 days of culture and injected out of the syringe. Then after 6 h of incubation following the injection process, cell viability was analyzed via live/dead staining and CCK-8 assay. For live/dead staining, calcein-AM and propidium iodide were mixed at a 1:1.5 ratio with 1 mL PBS. The samples were stained with staining solution for 15 min at room temperature and visualized by fluorescence microscopy. Dead cells appeared as red fluorescence, and green for live cells. The same concentration of SHEDs was digested to obtain a cell suspension after 3 days of culture, with injection and non-injection operations, respectively, live/dead staining was performed either.

### 2.9. In vitro odontogenic differentiation of SHEDs

SHEDs were seeded at a density of $5 \times 10^4$ cells per well on TCPs, 2 mg CMS or SMS, which were dispersed in 12-well plates with PM/OM for 7 days. Regular medium changes were performed every 2 days. PM was set as negative control. ARS staining was performed to test mineralized nodules formation. DMP-1 and DSPP genes expression were detected via RT-PCR. Immunofluorescent staining of DMP-1 and DSPP was conducted to detect the level of protein production.

### 2.10. In vitro angiogenic potential of SHEDs

SHEDs were cultured at a density of $5 \times 10^4$ cells per well on TCPs, 2 mg CMS or SMS respectively, and dispersed in 12-well plates with α-MEM medium for 7 days. Regular medium changes were performed every 2 days. VEGF and VEGF-R2 genes expression were detected via RT-PCR.

A Scratch test was conducted to test the effect of SHEDs loaded SMS on HUVECs migration. The procedure was described as aforementioned, after mechanically scratching the straight line to the monolayer cells, the culture medium from SHEDs, SHEDs loaded CMS (SHEDs/CMS) and SHEDs loaded SMS (SHEDs/SMS) were centrifuged respectively and the supernatant medium (conditioned medium) of each group was extracted and added to the well. Images were taken by light microscopy from random fields of each well after 24 h of observation. Migrating distance was analyzed using Image J software.

In vitro matrigel angiogenesis assay and chorioallantoic membrane (CAM) assay were used to examine the angiogenic potential of SHEDs after loading on CMS and SMS for 3 days. Briefly, HUVECs ($0.6 \times 10^4$ cells/300 μL) were suspended in SHEDs, SHEDs/CMS and SHEDs/SMS conditioned medium and then seeded in 24 well plate precoated with Matrigel (300 μL/well). Images were taken after 6 h culture and analyzed by Image J software.

For the CAM assay, fertilized chicken eggs were incubated at 38.3 °C for the first three days and 38.5 °C in the following two days in a humidified atmosphere. After 5 days, a small opening hole was made in the shell, and the CAM was exposed to the conditioned medium of SHEDs, SHEDs/CMS and SHEDs/SMS. The opening hole was covered by sterilized parafilm before the eggs were returned to the incubator. Five days later, the CAM was carefully dissected out of the eggs to assess angiogenesis. Pictures were taken with a stereomicroscope to quantify angiogenesis, and neovascular blood vessel branches were counted independently 2 times in a double-blind fashion.

### 2.11. In vivo SHEDs loaded SMS injection

Balb/C nude mice (male, 6-weeks old, 25 g average body weight) were used as subcutaneous injection models (LA2020393) and were randomly divided into five groups (Table S3). In brief, surgeries were performed under anesthesia in a sterile environment, SHEDs suspension, CMS, SMS, SHEDs/CMS, SHEDs/SMS were pre-cultured for 3 days and injected through 26 G syringe respectively on both sides of the subcutaneous dorsal pockets. Whole regenerating tissue specimens containing the cell loaded microspheres were explanted and fixed in 10% formalin four weeks after implantation. Specimens were decalcified in 17% ethylenediamine tetraacetic acid (EDTA) solution. The decalcified samples were trimmed, dehydrated with gradient ethanol, and embedded in paraffin. A series of slices (5 μm) were cut from the center of the repair site and stained with H&E and immunohistochemistry (DMP-1, DSPP and CD31) in accordance with standard protocols. All histological sections were observed using a light microscope.

### 2.12. In vivo SHEDs loaded SMS tooth segments implantation

Freshly extracted single rooted premolars were collected from healthy patients aged 15 to 30 y in the Oral and Maxillofacial Surgery Clinic at Peking University School and Hospital of Stomatology with informed consent and institutional review board approval (PKUSSIR-201734036). Tooth root segments were obtained from the middle third of the total root and made 2–3 mm in orifice width by using sterilized 330 and fissure burs. After removing the residual soft tissues, the roots were soaked in 17% EDTA at room temperature for 10 min and in 19% citric acid for 1 min to remove the smear layer. Next, the roots were treated with hydrogen peroxide for 5 min and 5.25% NaClO for 10 min for sterilization. Finally, the roots were rinsed with sterile PBS and incubated at 37 °C for 3–7 days to remove the residual disinfection agents [41]. Subcutaneous pockets were created using blunt dissection on the anesthetic nude mice (LA2020393). Root segments were firstly implanted into the dorsal pockets of nude mice, and SHEDs suspension, SHEDs/SMS were then injected into the root segments. After placement of the construct, the incisions were closed with suture. The animals were sacrificed, and samples were retrieved after 1 month of implantation. The samples were fixed in 4% formaldehyde for 24 h, decalcified with 10% EDTA, and processed for histological and immunohistochemical analyses.

### 2.13. Statistical analysis

All quantitative data were expressed as the mean ± standard deviation (SD) for n ≥ 3. Statistical analysis was carried out using one-way/two-way analysis of variance (ANOVA) with Tukey's test. Differences between groups of *$p < 0.05$ were considered statistically significant, **$p < 0.01$ and ***$p < 0.001$ were considered highly significant.

## 3. Results

### 3.1. Effect of SIM on SHEDs biological properties

To determine whether SIM exerted pro-odontogenic differentiation on SHEDs, we first screened the suitable dose range with no inhibitory effect on SHEDs proliferation and then selected optimized dose of SIM for SHEDs odontogenesis. As shown in Fig. 1a, a significant reduction in the absorbance values was observed for the SHEDs stimulated with SIM at 10 μM after seven days of culture. By light microscope observation, large quantities of dead cells were found in the 10 μM SIM stimulated group (Fig. S1). At 0.01–1 μM, SIM showed no inhibitory effect on SHEDs vitality. SHEDs are fully stretched and maintained similar spindle shape in

TCPs. The highest absorbance values were found in the 0.01 μM SIM group after 5 days of culture, whereas after subsequent two days of culture, there was no significant difference between 0.01 μM and 0.1 μM groups. Hence, a low concentration (0.01–1 μM) of SIM with no inhibitory effect on SHEDs proliferation was chosen for further experiments. Within 0.01–1 μM concentration range, stronger ALP and ARS staining were observed on visual inspection (Fig. 1b, Fig. S2). In particular, 0.01 μM SIM significantly enhanced SHEDs mineralized deposit formation (*$P$ < 0.05) (Fig. 1c), as well as the strongest DMP-1 and DSPP expression after induction for 7 days (Fig. 1 d-e). SIM exhibited a dose dependent effect on SHEDs angiogenesis and chemokine-related genes expression. SHEDs stimulated by 0.01 μM SIM showed the highest angiogenic (VEGF and VEGF-R2) gene and chemokine (SDF-1α and CXCR-4) genes
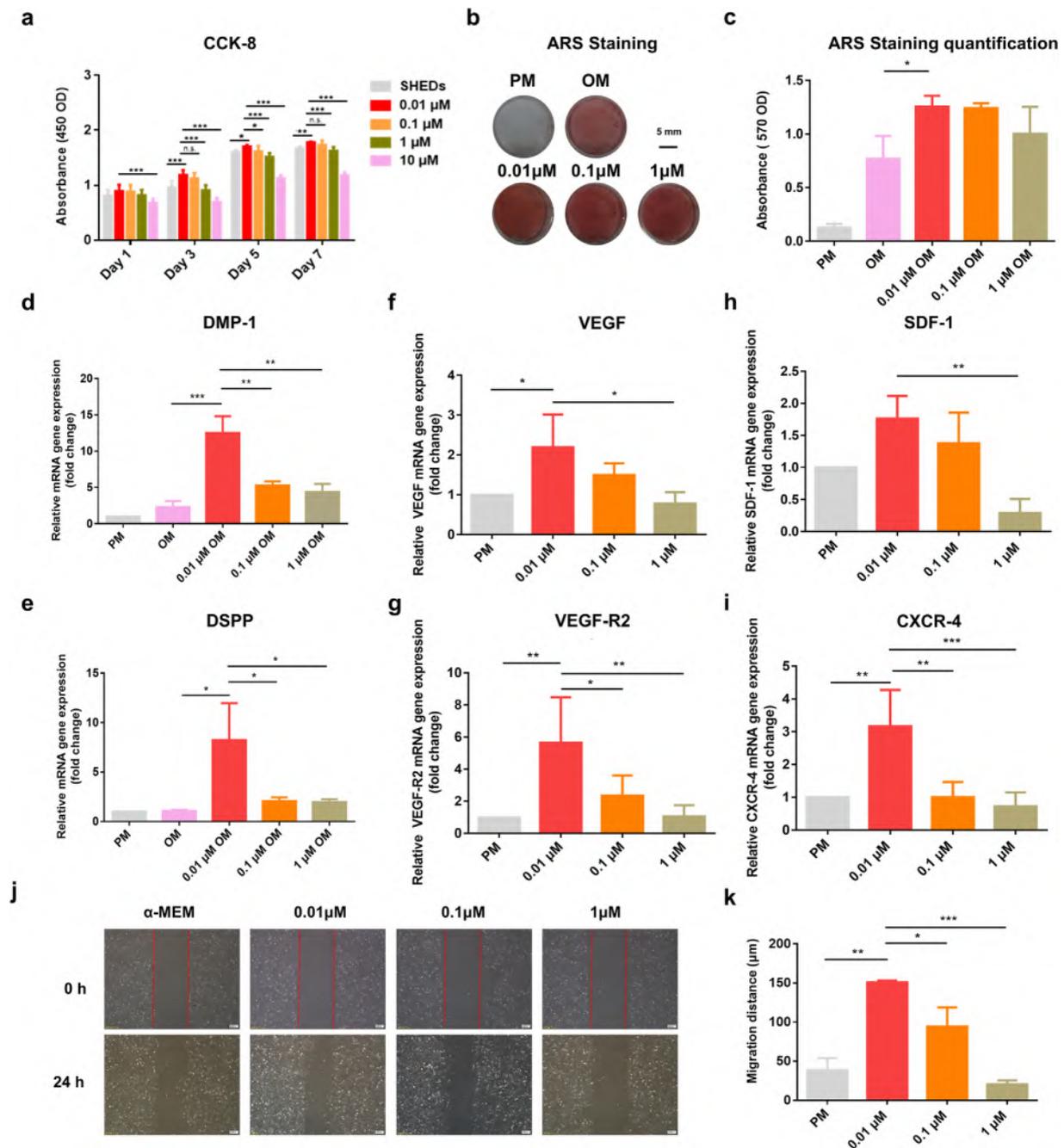


**Fig. 1.** (a) CCK-8 assay for SHEDs cultured in gradient concentrations of SIM. (b, c) Alizarin red S staining and quantitative analysis. (d, e) Odontogenic related genes expression. (f, g) Effects of 0.01–1 μM SIM on SHEDs angiogenesis-related genes expression. (h, i) chemokines related genes expression. (j, k) Effects of 0.01–1 μM SIM stimulated SHEDs conditioned medium on HUVECs migratory ability. Scale bar = 200 μm *$P$ < 0.05, **$P$ < 0.01, ***$P$ < 0.001.

expression (Fig. 1 f-i). With increasing SIM concentration, the expression levels of angiogenic and chemokine gene in SHEDs decreased gradually. At the concentration of 1 μM, the genes expression in SHEDs were the lowest. As shown in Fig. 2 j-k, the migratory distance of HUVECs was significantly increased in the 0.01 μM and 0.1 μM SIM stimulated SHEDs conditioned medium groups. Moreover, HUVECs migrated more distance in 0.01 μM SIM stimulated SHEDs conditioned medium group. When treated with 1 μM SIM stimulated SHEDs conditioned medium, HUVECs exhibited reduced mobility. Hence, 0.01 μM SIM was selected as the optimal bioactive dose for subsequent microsphere fabrication.

### 3.2. Fabrication and characterization of CMS and SMS

Herein, GelMA hydrogel microspheres (HMS) and cryogel microspheres (CMS) with different pore sizes (CMS-0, CMS-30 and CMS-60) were fabricated (Table S2). After loading with SHEDs, CMS-30 with an average pore size of ~15.5 μm showed the highest absorbance values during 7 days of culture (Fig. S3a) with more pseudopodia formation (Fig. S3b) and maintained strong green fluorescence before and after the injection process (Fig. S4), which indicated that CMS-30 is superior for SHEDs adhesion, proliferation, and cell protection. Therefore, the same gradient cooling procedure was selected for subsequent SMS fabrication (Fig. 3a). As shown in Fig. 3b, both CMS and SMS showed porous structures with spherical shapes and similar particle sizes and pore size distributions of ~95 μm and ~14 μm, respectively (Fig. S5). On the surface of SMS, well-dispersed PLGA/SMS nanoparticles can be observed (Fig. 2b), and the average size of PLGA/SIM nanoparticles is ~578 nm (Fig. S5). The degradation test showed that SMS degraded 73.92% within 12 h in 2 U/mL collagenase solution (Fig. 2c). The drug loading rate and encapsulation efficiency of SMS were 0.0118% and 93%, respectively. The cumulative release profile of SIM from SMS over a period of 29 days is shown in Fig. 2d. SIM maintained a sustained release with an average concentration of 0.0082 μM/day after the initial burst release on the first seven days (the maximum burst release of SIM was detected at day 1 with a concentration of 0.072 μM), which was close to the selected SIM concentration of 0.01 μM.

### 3.3. Proliferation, adhesion and post-injection vitality of SHEDs loaded SMS

As shown in Fig. S6a, SHEDs (green) were evenly dispersed in SMS. With prolonged culture time (7 days), SHEDs block together gradually (Fig. S6b) due to the secreted extracellular matrix. The proliferation of SHEDs cultured on CMS and SMS was determined by CCK-8 assay as shown in Fig. 3a. Compared with TCPs, SHEDs cultured on CMS and SMS showed higher optical values after 7 days of culture, which was attributed to the porous structure of microspheres. The highest optical values were detected in the SMS group, owing to the sustained release of SIM that promotes SHEDs proliferation. SHEDs showed a polygonal morphology with multiple stretched prolongations on the CMS and SMS surfaces (Fig. 3b). Additionally, as shown in fluorescent images (Fig. S7), some of the red fluorescent signals (SHEDs cytoskeleton) were overlaid by the green fluorescent signals (microspheres), which indicated that SHEDs could grow into the pore walls of microspheres. Although SHEDs loaded on microspheres showed no obvious difference in cell morphology, the adhesion marker gene expression (ITG-β) was higher in the SMS group (Fig. 3c), which is in consistent with the immunofluorescence detection results (Fig. 3d) that stronger green fluorescence (vinculin protein) was observed in SHEDs/SMS. As shown in Fig. 3e and f, CMS and SMS had large amounts of living cells with green fluorescence after 3 days preculture, which was in accordance with the optical values. However, a number of dead cells were stained with red fluorescence in SHEDs suspension injection group (Fig. S8), indicating that the injection operation induced cell apoptosis. 6 h after injection, due to the tight attachment of SHEDs on SMS surface, the green fluorescence and optical values decreased much less in the SMS group, which demonstrated the
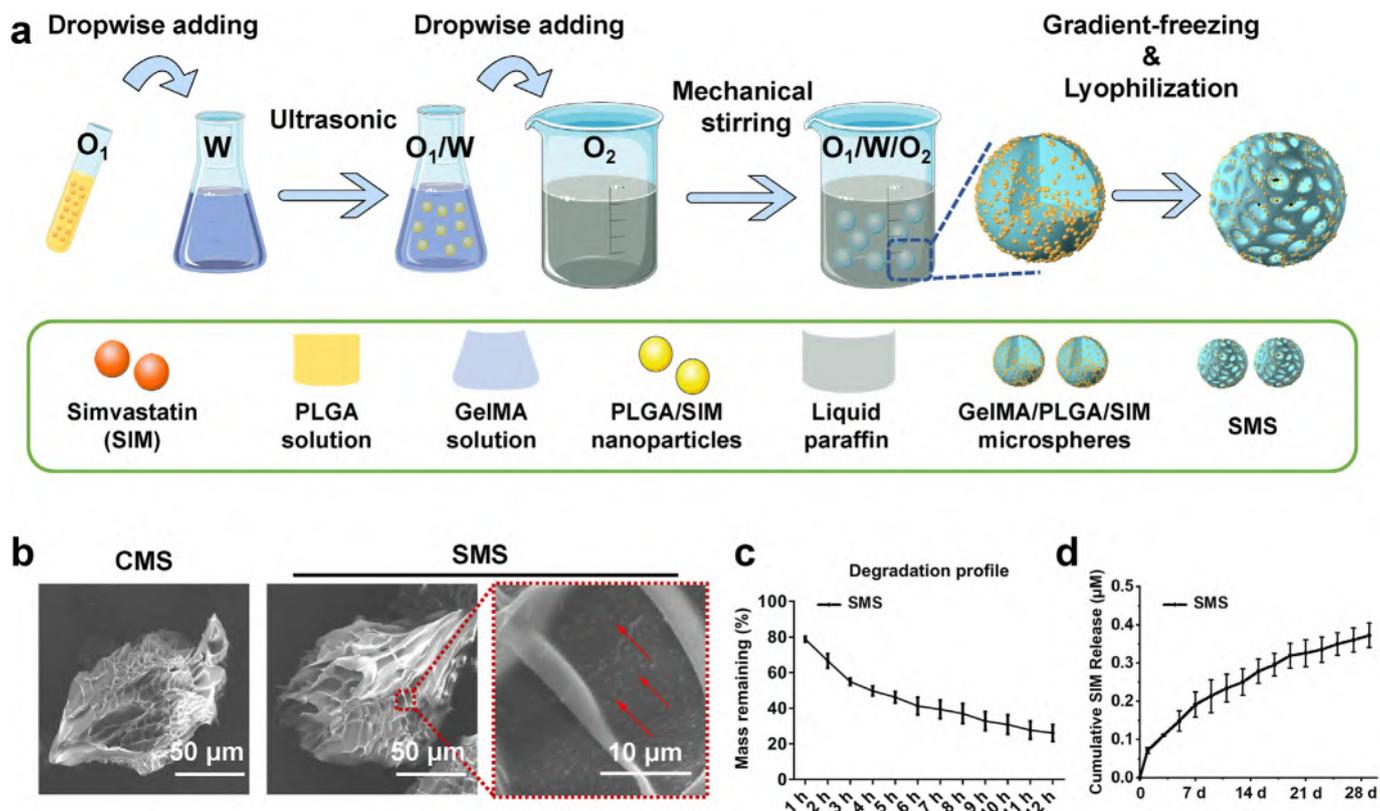


**Fig. 2.** (a) Infographics of the fabrication of SMS. (b) SEM images of CMS and SMS. Red arrows indicate PLGA nanoparticles. (c) Degradation profile of SMS in 2 U/mL collagenase solution detected at preselected time points. (d) Cumulative release profile of SIM from SMS within the experimental period of 29 days in PBS at 37 °C.
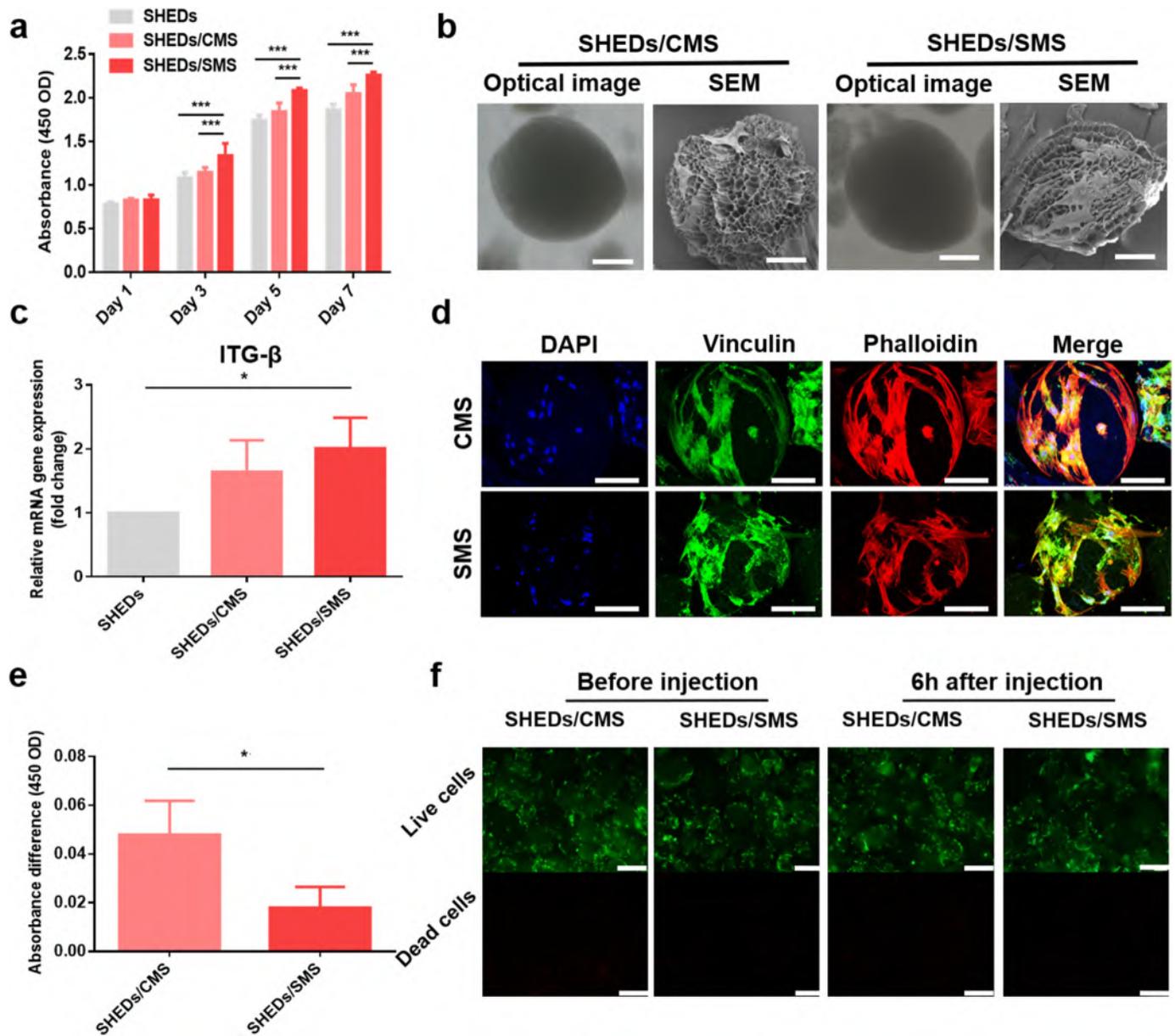
**Fig. 3.** (a) CCK-8 assay for SHEDs proliferation on TCPs, CMS and SMS in 7 days of culture. (b) Light microscopy and SEM images of SHEDs loaded on CMS or SMS. Scale bars = 40 μm. (c) ITG-β1 gene expression. (d) CLSM images of SHEDs loaded on CMS or SMS, nuclei stained with DAPI (blue), vinculin protein (green) and cytoskeleton stained with phalloidin (red). Scale bars = 40 μm. (e) The absorbance difference of SHEDs loaded on CMS and SMS before and 6 h after the injection process. (f) Fluorescence images of living (green) and dead (red) SHEDs on CMS or SMS before and after the injection process. Scale bars = 100 μm.

excellent cell protection ability of SMS. Altogether, SMS is a suitable microcarrier for SHEDs delivery due to the enhanced adhesion, proliferation and cell protection properties.

### 3.4. The odontogenic effects of SMS on SHEDs

We hypothesized that SMS with sustained release of SIM could provide an odontogenic environment for SHEDs. As shown in Fig. 4a, ARS staining suggested that SHEDs cultured on CMS and SMS exhibited more mineral deposits than OM group after induction for 7 days. DMP-1 and DSPP genes expression were remarkably upregulated, with a more than 3-fold increase in SHEDs/SMS compared to SHEDs/CMS (*$P < 0.05$) (Fig. 4b and c). As shown in CLSM images (Fig. 4d and e), when cultured in PM, SHEDs showed weak green fluorescent signals, which indicated lower DMP-1 and DSPP protein production. In contrast, when induced by OM, SHEDs, SHEDs/CMS and SHEDs/SMS showed varied intensity of fluorescence signals on DMP-1 and DSPP protein production, weakest for

TCPs group and strongest for SHEDs/SMS group (Fig. S9). Overall, SMS promoted SHEDs odontogenic differentiation potential in an odontogenic induced microenvironment.

### 3.5. Pro-angiogenic potential of SMS on SHEDs and HUVECs

As shown in Fig. 5a and b, SHEDs loaded on SMS showed higher VEGF and VEGF-R2 genes expression than CMS and control group after 7 days of culture (*$P < 0.05$ or ***$P < 0.001$). The scratch test (Fig. 5c and d) revealed the influence of different conditioned media (SHEDs, SHEDs/CMS, SHEDs/SMS) on the migratory ability of HUVECs. The migratory distance of HUVECs was significantly increased in the SHEDs/CMS and SHEDs/SMS groups as compared to SHEDs group. However, no significant difference was found between the SHEDs/SMS group and SHEDs/CMS group in migration distance. Nevertheless, compared with the CMS and TCPs group, SHEDs cultured on SMS significantly increased the number of meshes, nodes, segments, (Fig. S10) formation and showed
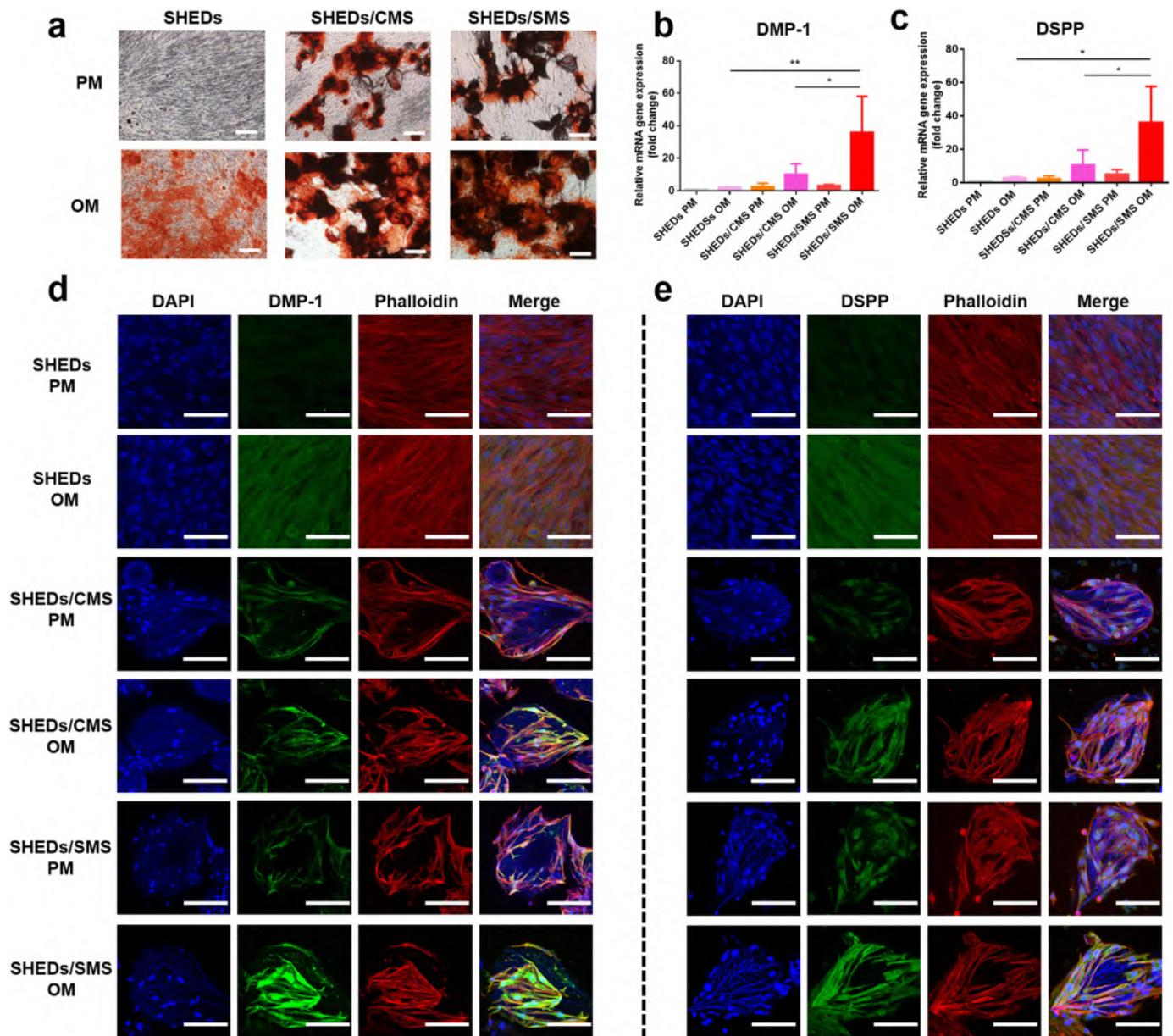
**Fig. 4.** (a) ARS staining of SHEDs cultured on different substrates with PM/OM medium for 7 days. Scale bars = 100 μm (b) DMP-1 and (c) DSPP genes expression detected by RT-PCR, (d) DMP-1 and (e) DSPP production detected by CLSM images. Green fluorescence indicates DMP-1 or DSPP, red fluorescence indicates actin fibers, and blue fluorescence indicates nuclei. Scale bars = 50 μm.

higher total tube length (Fig. 5e and f) in HUVECs network structures (*$P < 0.05$ or **$P < 0.01$ or ***$P < 0.001$). Furthermore, CAM experiments demonstrated that SHEDs loaded on SMS formed higher numbers of vessels. (***$P < 0.001$). Taken together, the sustained release of SIM in SMS promoted SHEDs angiogenic potential and remarkably enhanced HUVECs angiogenesis.

### 3.6. Subcutaneous injection of SHEDs/SMS

As shown in Fig. 6, the directly injected SHEDs suspension group formed few amounts of neonatal tissue and vessels because of low cell retention. However, nude mice injected with CMS or SMS regenerated orderly arranged tissues with dense fiber-like structures. No inflammatory cells were found in either group, which confirms the excellent biocompatibility of GelMA. By H&E and immunohistochemical staining,

although there were more blood vessels in the SMS group, no obvious CD31 positive cells were found because the antibody targeted human derived cells, which illustrated the angiogenic regulatory effect of SMS on host tissues. In addition, there are some gaps between microspheres and circumambient tissues after the histologic sectioning process, which illustrates the lack of tissue integration ability of materials in the absence of other bioactive factors. After introducing SHEDs into the implants, CMS and SMS were tightly integrated with the surrounding tissues and grafted cells could be found in the pores of microspheres. The overview of the SHEDs/CMS and SHEDs/SMS implants are pink in color, which indicated the in-growth blood vessels. Most of vascular networks were formed around the microspheres in the SHEDs/SMS group, and the highest numbers of CD31, DMP-1 and DSPP positive cells were found. The subcutaneous results indicated that the sustained release of SIM from SMS would promote SHEDs odontogenic and angiogenic potential, and
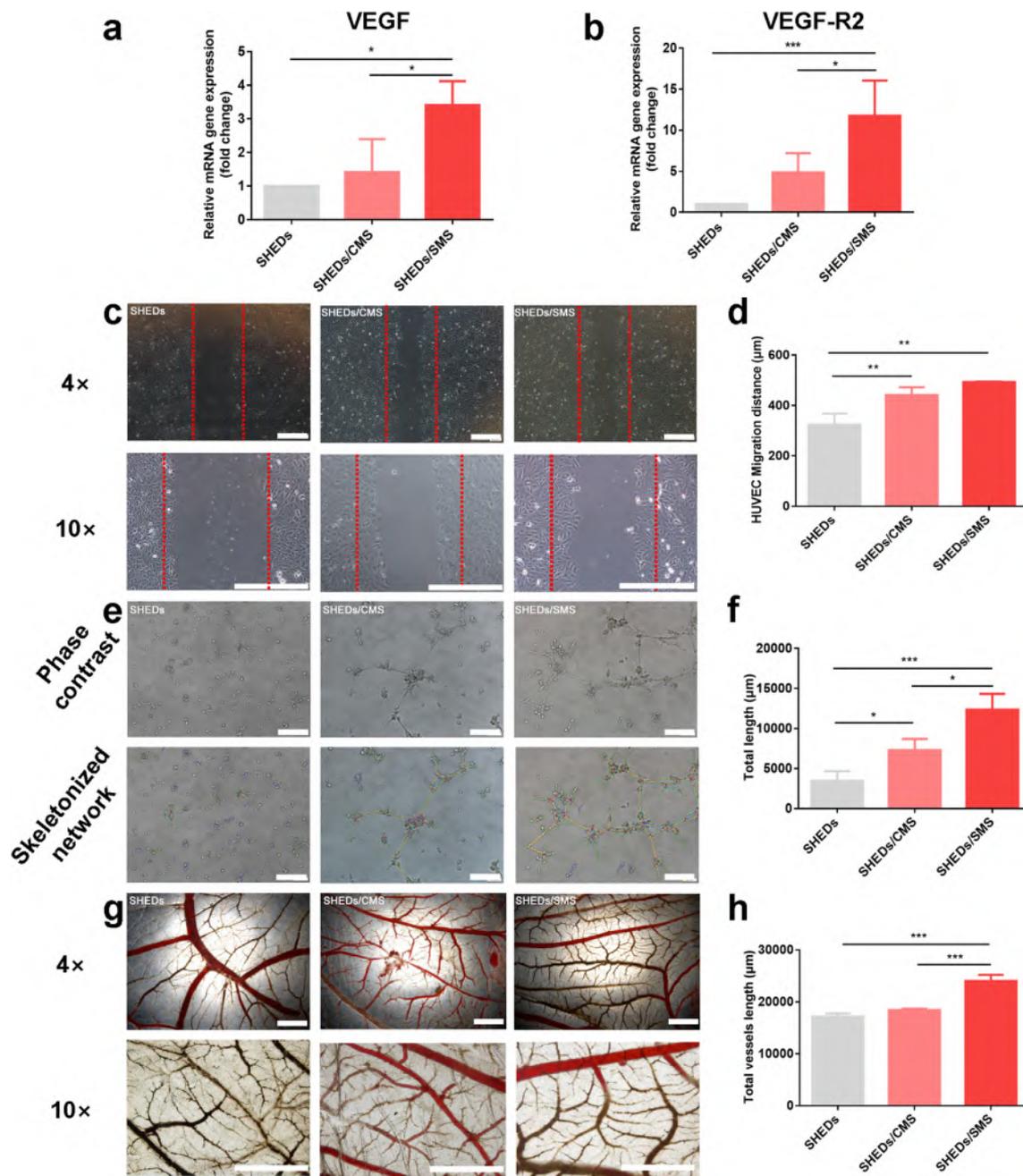
**Fig. 5.** RT-PCR analysis for VEGF (a) and VEGF-R2 (b) genes expression in SHEDs. (c, d) HUVECs migration cultured in conditioned medium (SHEDs, SHEDs/CMS and SHED/SMS) and corresponding quantitative analysis of migration distance. (e, f) In vitro tubule formation of HUVECs induced by conditioned medium (SHEDs, SHEDs/CMS and SHED/SMS) and the corresponding quantitative analysis of total tubules length. (g. h) CAM assay for neovascular formation evaluation and corresponding quantitative analysis of total vessels length. Samples were stimulated with SHEDs, SHEDs/CMS or SHED/SMS conditioned medium. Scale bars = 400 μm.

the SHEDs/SMS constructs would be capable of regenerating highly organized vascularized tissue.

### 3.7. Subcutaneous implantation of SHEDs/SMS injected tooth segments

To further mimic the tooth microenvironment, SHEDs/SMS were injected into tooth root canals and implanted into nude mice (Fig. 7a). SHEDs suspension injected group was used as a negative control. The implantation of SHEDs/SMS injected tooth segments caused no inflammatory response in the liver, kidney and spleen of nude mice (Fig. S11), which indicated biocompatibility of the engraftments. As shown in Fig. 7b, little tissue regenerated in control group. The newly formed tissues showed no close integration with the inner dentin tubules and no

structures similar to those of odontoblastic layers were observed by H&E and Masson staining. However, higher amounts of collagenous vascularized connective tissues were formed in the SHEDs/SMS group. In the interface of regenerated soft tissue and inner dentin are the linear arrangement cells concentrated on the border of the inner dentin wall, and their processes penetrated into the dentinal tubules. The cells stained in dark brown indicated positive DMP-1 and DSPP staining, similar to the odontoblastic cells in native dental pulp tissues, suggesting that SMS loaded with SHEDs could regenerate vascularized pulp-like tissue in tooth root canals. Moreover, vascular networks regenerated in the soft tissues (Fig. S12), with higher numbers of CD31 positive cells around vessel tubules and microspheres compared with the negative control (Fig. 7c).
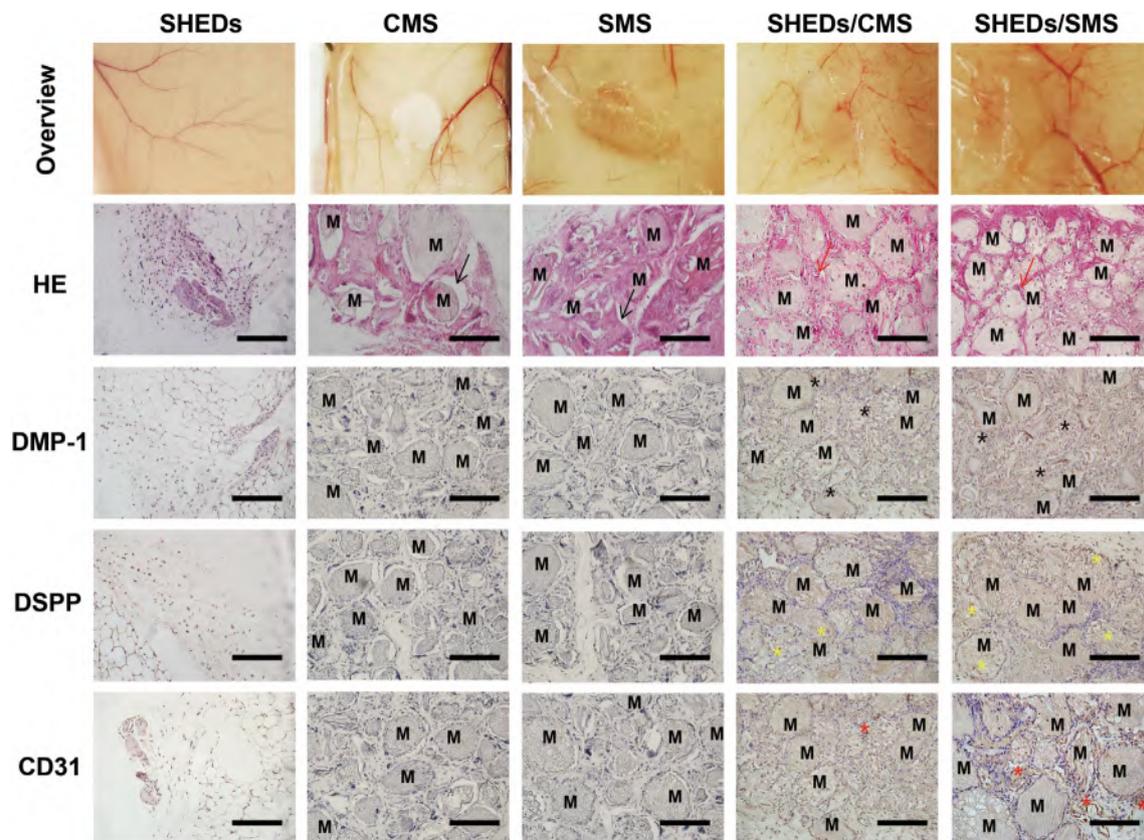
**Fig. 6.** Histological evaluations (H&E staining) and CD31, DMP-1 and DSPP immunohistochemical staining at 1 month after each group being subcutaneously injected into nude mice back. The black arrows indicate the gap between microspheres and connective tissues, red arrows indicate newly formed vessels, black stars indicate the DMP-1 positive cells, yellow stars indicate DSPP positive cells, red stars indicate CD31 positive cells, and M represents the location of residual microspheres. Scale bars = 100 μm.

## 4. Discussion

Dental derived stem cells play a substantial role in promoting pulp regeneration, nevertheless, stem cells have limited capacity to differentiate into the desired phenotype in devitalized root canals [42,43]. Dental pulp tissue is enclosed within the calcified tooth root canals with apical foramen the only access to peripheral tissues, and it is difficult to regenerate blood vessels by relying solely on the angiogenic ability of dental derived stem cells [44]. Recruitment of endothelial cells contributes to the formation of dental pulp with a rich vasculature network similar to that of native dental pulp [45]. Here, 0.01 μM SIM was shown to facilitate the differentiation of SHEDs into highly secretive odontoblast-like cells with high odontogenic genes expression. Particularly, at this dosage, SIM showed pleiotropic effects that promoted SHEDs proliferation and enhanced angiogenic and chemokine genes expression. Accordingly, SIM stimulated SHEDs conditioned medium effectively improved HUVECs migration distance, which was regulated through the SDF-1/CXCR-4 axis [46]. The administration of SIM in the construction of pulp regeneration microenvironment would be a simple and effective way to regulate SHEDs biological behavior in multiple ways.

The root canals featured with unique anatomical structures, which are slender and irregular in shape. Although bulk scaffolds could improve the cell retention rate by providing three dimensional (3D) support for stem cell growth and differentiation, they scarcely fit root canals [47,48]. In addition, the injection of stem cells through thin syringe needles brings up multiple pressures and collisions, which can induce cell apoptosis [40]. Here, GelMA CMS was fabricated as injectable 3D macroporous biomimetic scaffolds for SHEDs delivery. The interconnected porous structure of CMS possesses more oxygen and nutrient exchange for SHEDs vitality maintenance [49]. The tuned porous structure of scaffolds

could modulate the morphology and proliferation of stem cells [50–52]. In our study, CMS-30 with average pore size of 14 μm endowed SHEDs with grow into the porous walls which contributed to the enhanced proliferation capacity and exhibited CMS cell protection potential during the injection process.

In addition, cryogels also act as delivery vehicles for sustained signalling molecule release [53]. To induce SHEDs phenotypes in situ, we constructed a multilevel SIM sustained release system. First, SIM is released from PLGA nanoparticles into the GelMA matrix and then diffuses to the circumambient environment. As expected, SMS exhibited a sustained SIM release profile for approximately one month. SHEDs loaded on SMS expressed higher levels of adhesion marker expression and promoted proliferation capacity. The porous structure of SMS and enhanced cell adhesion capacity endow SHEDs with a higher level of vitality after the injection process. Under an odontogenic induced microenvironment, SHEDs stimulated with SIM elicited an odontoblastic phenotype that showed significantly higher levels of DMP-1 and DSPP gene and protein expression, along with an increase in mineralized nodule deposition. In addition, the sustained release of SIM promoted SHEDs angiogenic genes expression, thus effectively promoting HUVECs migratory ability, tubule formation potential and CAM neovascular regeneration capacity. The ectopic subcutaneous implantation of such cell-carrier constructs identified the biological properties of scaffold and define the multipotent functions of grafted cells [40]. The in vivo delivery of SHEDs suspension showed a lower amount of tissue formation due to low cell retention and survival rate. SHEDs loaded on microspheres have effectively improved complex integration potential with host tissues, which was in accordance with a previous report demonstrating that the administration of stem cells would enhance scaffolds host tissue integration in vivo [54]. The injected SHEDs/SMS constructs successfully
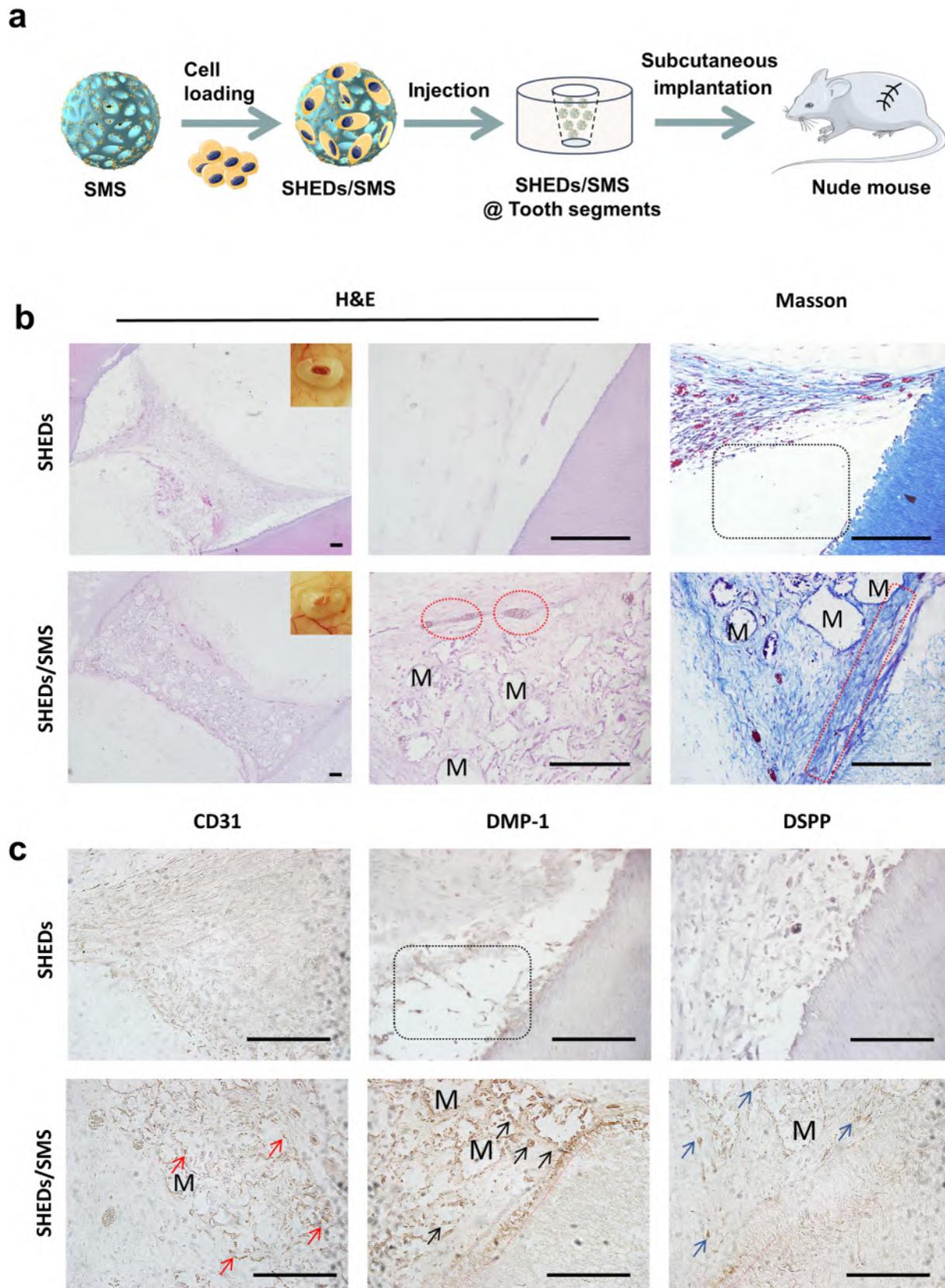
**Fig. 7.** (a) Infographics of the *in vivo* implanting process. (b) Dental pulp-like tissue regeneration through SHEDs, SHEDs/SMS combined with human root segments after implantation subcutaneously into nude mice for 1 month. The black-dotted frames indicate the gaps between regenerated tissue and tooth root segment, red-dotted circles indicate vessels, the red-dotted frames indicate odontoblastic layer, the red arrows indicate CD31 positive cells, black arrows indicate the DMP-1 positive cells, blue arrows indicate DSPP positive cells, the red dotted lines indicate cell processes penetrated into the dentin tubules. M represents the location of residual microspheres. Scale bars = 100 μm.

formed more vascularized tissue with an odontoblastic cell like phenotype in nude mice, thereby proving the feasibility of SMS cell loading and a SIM release system for vascularized pulp regeneration.

Tooth root segments possess unique dentin tubule structures that could regulate stem cells odontogenic differentiation. Moreover, the inner toot canal wall of dentin tubules contains versatile growth factors that can be released after EDTA treatment. The tooth segments provide a physical and chemical environment for the implanted complex during the regenerating process [55–57]. In our study, SHEDs and SHEDs/SMS were injected into tooth segments to explore the effect of pulp regeneration in nude mice. More dental pulp-like tissue with abundant blood vessels was generated in the SHEDs/SMS group than in the SHEDs suspension group under the condition of similar amounts of implanted cells. Although Masson staining showed vascularization in SHEDs suspension group, CD31 positive cells could hardly be found in this group, thus proving that the neovessels were regenerated by mouse host tissue. The application of SMS can effectively improve the retention rate of SHEDs *in vivo* and provide three-dimensional structural support for SHEDs, which is conducive to tissue formation. Close to the inner root canal walls, the linearly arranged cells stretched their processes into the dentinal tubules, and cells in this layer showed positive DMP-1 and DSPP staining, which are similar to the structure of the odontoblastic layer, proving that SHEDs/SMS can effectively promote the formation of dental pulp-dentin complexes. CD31 positive cells existed not only in neovessels but also near the microspheres, which indicated that the sustained release of SIM further promotes SHEDs angiogenic potential. In addition, SMS would be safe for *in vivo* application due to the biocompatibility verified by the lack of inflammatory aggregation in the main organs of nude mice.

In the present study, the sustained release of SIM from GelMA cryogel microspheres with multiple favourable effects (enhanced proliferation, adhesion, angiogenic potential and odontogenic differentiation) could provide a simplified method for constructing a native microenvironment. Our study preliminarily demonstrated the feasibility of SHEDs loaded SMS in regenerative endodontic applications. In clinical trials, there will still have residual bacteria resides in the dentin tubules after mechanical cleaning treatment, persisted inflammation may hamper the regenerative processes and will eventually lead to pulp necrosis [58]. SIM has been demonstrated to show anti-inflammatory potential [59,60], it is meaningful to further explore the anti-inflammatory effect of SIM on SHEDs in this biomimetic 3D tissue engineering scaffold [61]. Considering further clinical translation, the construct should be injected into full length root canals sealed with optimal seal materials to explore the regenerative capacity *in vivo*, and in situ experiments on large animals with comparable "anatomical, physiologic, histologic, and pathologic characteristics to clinical situations" should be taken into account in future work [41, 62–64].

## 5. Conclusion

In this work, for the first time, we found that 0.01 μM SIM could promote the odontogenic differentiation and angiogenic potential of SHEDs. To effectively deliver SHEDs and SIM to irregularly shaped narrow root canals, a kind of injectable simvastatin functionalized GelMA cryogel microspheres loaded with SHEDs was constructed. These microspheres provided feasibility to promote SHEDs adhesion, proliferation, and cell protection during the injection process. Attributed to the sustained release of SIM, SHEDs loaded SMS showed enhanced odontogenic and proangiogenic potential *in vitro* and regenerated vascularized pulp-like tissue *in vivo*, exhibiting promising applications in endodontic regenerative dentistry.

## Credit author statement

**Xiaojing Yuan**: Conceptualization, Investigation, Methodology, Formal analysis, Writing – original draft, **Zuoying Yuan**: Conceptualization, Investigation, Methodology, Writing – original draft, **Yuanyuan Wang** Formal analysis, **Zhuo Wan**: Investigation, **Xiaotong Wang:** Resources, **Qing Cai**: Writing – review & editing, **Yuming Zhao**: Supervision, Data curation, **Shi Yu**: Resources, **Jianmin Han**: Resources, **Jianyong Huang**: Writing – review & editing, **Chunyang Xiong**: Project administration, **Lihong Ge**: Supervision, Funding acquisition

## Data availability

The raw/processed data required to reproduce these findings cannot be shared at this time as the data also forms part of an ongoing study.

## Declaration of competing interest

The authors declare no conflicting financial or other competing interests in this research.

## Acknowledgements and funding statements

## Appendix A. Supplementary data

Supplementary data to this article can be found online at https://doi.org/10.1016/j.mtbio.2022.100209.

## References

[1] W. Zhang, P.C. Yelick, Vital pulp therapy-current progress of dental pulp regeneration and revascularization, Int J Dent 2010 (2010) 856087.
[2] D. Ricucci, J.F. Siqueira Jr., S. Loghin, L.M. Lin, Pulp and apical tissue response to deep caries in immature teeth: a histologic and histobacteriologic study, J. Dent. 56 (2017) 19–32.
[3] M.V. Korolenkova, M.S. Rakhmanova, [Outcomes of traumatic dental injuries in children], Stomatol. 98 (4) (2019) 116–122.
[4] G. Schmalz, M. Widbiller, K.M. Galler, Clinical perspectives of pulp regeneration, J. Endod. 46 (9S) (2020) S161–S174.
[5] M. Cvek, Prognosis of luxated non-vital maxillary incisors treated with calcium hydroxide and filled with gutta-percha. A retrospective clinical study, Endod. Dent. Traumatol. 8 (2) (1992) 45–55.
[6] L. Ling, Y.M. Zhao, X.T. Wang, Q. Wen, L.H. Ge, Regeneration of dental pulp tissue by autologous grafting stem cells derived from inflammatory dental pulp tissue in immature premolars in a beagle dog, Chin. J. Dent. Res. 23 (2) (2020) 143–150.
[7] X. Zhu, J. Liu, Z. Yu, C.A. Chen, H. Aksel, A.A. Azim, G.T. Huang, A miniature swine model for stem cell-based de novo regeneration of dental pulp and dentin-like tissue, Tissue Eng. C Methods 24 (2) (2018) 108–120.
[8] X. Zhang, H. Li, J. Sun, X. Luo, H. Yang, L. Xie, B. Yang, W. Guo, W. Tian, Cell-derived micro-environment helps dental pulp stem cells promote dental pulp regeneration, Cell Prolif 50 (5) (2017).
[9] E. Piva, S.A. Tarle, J.E. Nor, D. Zou, E. Hatfield, T. Guinn, E.J. Eubanks, D. Kaigler, Dental pulp tissue regeneration using dental pulp stem cells isolated and expanded in human serum, J. Endod. 43 (4) (2017) 568–574.
[10] Y. Itoh, J.I. Sasaki, M. Hashimoto, C. Katata, M. Hayashi, S. Imazato, Pulp regeneration by 3-dimensional dental pulp stem cell constructs, J. Dent. Res. 97 (10) (2018) 1137–1143.
[11] R. Kunimatsu, K. Nakajima, T. Awada, Y. Tsuka, T. Abe, K. Ando, T. Hiraki, A. Kimura, K. Tanimoto, Comparative characterization of stem cells from human exfoliated deciduous teeth, dental pulp, and bone marrow-derived mesenchymal stem cells, Biochem. Biophys. Res. Commun. 501 (1) (2018) 193–198.
[12] X. Wang, X.J. Sha, G.H. Li, F.S. Yang, K. Ji, L.Y. Wen, S.Y. Liu, L. Chen, Y. Ding, K. Xuan, Comparative characterization of stem cells from human exfoliated deciduous teeth and dental pulp stem cells, Arch. Oral Biol. 57 (9) (2012) 1231–1240.
[13] A.L. Junior, C.C.G. Pinheiro, D.Y.S. Tanikawa, J.R.M. Ferreira, M.T. Amano, D.F. Bueno, Mesenchymal stem cells from human exfoliated deciduous teeth and the orbicularis oris muscle: how do they behave when exposed to a proinflammatory stimulus? Stem Cell. Int. 2020 (2020) 3670412.
[14] M. Miura, S. Gronthos, M. Zhao, B. Lu, L.W. Fisher, P.G. Robey, S. Shi, SHED: stem cells from human exfoliated deciduous teeth, Proc. Natl. Acad. Sci. U. S. A. 100 (10) (2003) 5807–5812.

[15] M. Zhang, F. Jiang, X. Zhang, S. Wang, Y. Jin, W. Zhang, X. Jiang, The effects of platelet-derived growth factor-bb on human dental pulp stem cells mediated dentin-pulp complex regeneration, Stem Cells Transl Med 6 (12) (2017) 2126–2134.

[16] R. Zhang, L. Xie, H. Wu, T. Yang, Q. Zhang, Y. Tian, Y. Liu, X. Han, W. Guo, M. He, S. Liu, W. Tian, Alginate/laponite hydrogel microspheres co-encapsulating dental pulp stem cells and VEGF for endodontic regeneration, Acta Biomater. 113 (2020) 305–316.

[17] J.W. Yang, Y.F. Zhang, Z.Y. Sun, G.T. Song, Z. Chen, Dental pulp tissue engineering with bFGF-incorporated silk fibroin scaffolds, J. Biomater. Appl. 30 (2) (2015) 221–229.

[18] Y. Niu, Q. Li, Y. Ding, L. Dong, C. Wang, Engineered delivery strategies for enhanced control of growth factor activities in wound healing, Adv. Drug Deliv. Rev. 146 (2019) 190–208.

[19] B. Leader, Q.J. Baca, D.E. Golan, Protein therapeutics: a summary and pharmacological classification, Nat. Rev. Drug Discov. 7 (1) (2008) 21–39.

[20] A.W. James, G. LaChaud, J. Shen, G. Asatrian, V. Nguyen, X. Zhang, K. Ting, C. Soo, A review of the clinical side effects of bone morphogenetic protein-2, Tissue Eng. B Rev. 22 (4) (2016) 284–297.

[21] A.S. Tulbah, E. Pisano, E. Landh, S. Scalia, P.M. Young, D. Traini, H.X. Ong, Simvastatin nanoparticles reduce inflammation in lps-stimulated alveolar macrophages, J. Pharmacol. Sci. 108 (12) (2019) 3890–3897.

[22] D. Kirmizis, A. Papagianni, F. Dogrammatzi, G. Efstratiadis, D. Memmos, Anti-inflammatory effects of simvastatin in diabetic compared to non-diabetic patients on chronic hemodialysis, J. Diabetes 5 (4) (2013) 492–494.

[23] N.M. Al-Rasheed, N.M. Al-Rasheed, Y.A. Bassiouni, I.H. Hasan, M.A. Al-Amin, H.N. Al-Ajmi, A.M. Mahmoud, Simvastatin ameliorates diabetic nephropathy by attenuating oxidative stress and apoptosis in a rat model of streptozotocin-induced type 1 diabetes, Biomed. Pharmacother. 105 (2018) 290–298.

[24] J. Xu, X. Liu, J. Chen, A. Zacharek, X. Cui, S. Savant-Bhonsale, Z. Liu, M. Chopp, Simvastatin enhances bone marrow stromal cell differentiation into endothelial cells via notch signaling pathway, Am. J. Physiol. Cell Physiol. 296 (3) (2009) C535–C543.

[25] D.G. Soares, G. Anovazzi, E.A.F. Bordini, U.O. Zuta, M.L.A. Silva Leite, F.G. Basso, J. Hebling, C.A. de Souza Costa, Biological analysis of simvastatin-releasing chitosan scaffold as a cell-free system for pulp-dentin regeneration, J. Endod. 44 (6) (2018) 971–976 e1.

[26] B. Tyler, D. Gullotti, A. Mangraviti, T. Utsuki, H. Brem, Polylactic acid (PLA) controlled delivery carriers for biomedical applications, Adv. Drug Deliv. Rev. 107 (2016) 163–175.

[27] B.K. Lee, Y. Yun, K. Park, PLA micro- and nano-particles, Adv. Drug Deliv. Rev. 107 (2016) 176–191.

[28] Y. Zhang, H. Leng, Z. Du, Y. Huang, X. Liu, Z. Zhao, X. Zhang, Q. Cai, X. Yang, Efficient regeneration of rat calvarial defect with gelatin-hydroxyapatite composite cryogel, Biomed. Mater. 15 (6) (2020), 065005.

[29] K. Yue, G. Trujillo-de Santiago, M.M. Alvarez, A. Tamayol, N. Annabi, A. Khademhosseini, Synthesis, properties, and biomedical applications of gelatin methacryloyl (GelMA) hydrogels, Biomaterials 73 (2015) 254–271.

[30] Y. Hu, W. Dan, S. Xiong, Y. Kang, A. Dhinakar, J. Wu, Z. Gu, Development of collagen/polydopamine complexed matrix as mechanically enhanced and highly biocompatible semi-natural tissue engineering scaffold, Acta Biomater. 47 (2017) 135–148.

[31] K.Q. Huang, G.T. Liu, Z.P. Gu, J. Wu, Tofu as excellent scaffolds for potential bone regeneration, Chin. Chem. Lett. 31 (12) (2020) 3190–3194.

[32] T. Fang, Z. Yuan, Y. Zhao, X. Li, Y. Zhai, J. Li, X. Wang, N. Rao, L. Ge, Q. Cai, Synergistic effect of stem cells from human exfoliated deciduous teeth and rhBMP-2 delivered by injectable nanofibrous microspheres with different surface modifications on vascularized bone regeneration, Chem. Eng. J. 370 (2019) 573–586.

[33] L. Gu, J. Zhang, L. Li, Z. Du, Q. Cai, X. Yang, Hydroxyapatite nanowire composited gelatin cryogel with improved mechanical properties and cell migration for bone regeneration, Biomed. Mater. 14 (4) (2019), 045001.

[34] Z. Yuan, X. Yuan, Y. Zhao, Q. Cai, Y. Wang, R. Luo, S. Yu, Y. Wang, J. Han, L. Ge, J. Huang, C. Xiong, Injectable GelMA cryogel microspheres for modularized cell delivery and potential vascularized bone regeneration, Small 17 (11) (2021), e2006596.

[35] T. Yang, Q. Zhang, L. Xie, R. Zhang, R. Qian, Y. Tian, G. Chen, W. Tian, hDPSC-laden GelMA microspheres fabricated using electrostatic microdroplet method for endodontic regeneration, Mater Sci Eng C Mater Biol Appl 121 (2021) 111850.

[36] Y. Tao, K. Cai, S. Liu, Y. Zhang, Z. Chi, J. Xu, Pseudo target release behavior of simvastatin through pH-responsive polymer based on dynamic imine bonds: promotes rapid proliferation of osteoblasts, Mater Sci Eng C Mater Biol Appl 113 (2020) 110979.

[37] F. Qiao, J. Zhang, J. Wang, B. Du, X. Huang, L. Pang, Z. Zhou, Silk fibroin-coated PLGA dimpled microspheres for retarded release of simvastatin, Colloids Surf. B Biointerfaces 158 (2017) 112–118.

[38] Z. Yuan, P. Wei, Y. Huang, W. Zhang, F. Chen, X. Zhang, J. Mao, D. Chen, Q. Cai, X. Yang, Injectable PLGA microspheres with tunable magnesium ion release for promoting bone regeneration, Acta Biomater. 85 (2019) 294–309.

[39] Z. Yuan, Z. Wan, P. Wei, X. Lu, J. Mao, Q. Cai, X. Zhang, X. Yang, Dual-controlled release of icariin/Mg(2+) from biodegradable microspheres and their synergistic upregulation effect on bone regeneration, Adv Healthc Mater 9 (11) (2020), e2000211.

[40] D.X. Wei, J.W. Dao, G.Q. Chen, A micro-ark for cells: highly open porous polyhydroxyalkanoate microspheres as injectable scaffolds for tissue regeneration, Adv. Mater. 30 (31) (2018), e1802273.

[41] X. Li, C. Ma, X. Xie, H. Sun, X. Liu, Pulp regeneration in a full-length human tooth root using a hierarchical nanofibrous microsphere system, Acta Biomater. 35 (2016) 57–67.

[42] H. Zou, G. Wang, F. Song, X. Shi, Investigation of human dental pulp cells on a potential injectable poly(lactic-co-glycolic acid) microsphere scaffold, J. Endod. 43 (5) (2017) 745–750.

[43] H. Bakhtiar, M. Pezeshki-Modaress, Z. Kiaipour, M. Shafiee, M.R. Ellini, A. Mazidi, S. Rajabi, S. Zamanlui Benisi, S.N. Ostad, K. Galler, P. Pakshir, A. Azarpazhooh, A. Kishen, Pulp ECM-derived macroporous scaffolds for stimulation of dental-pulp regeneration process, Dent. Mater. 36 (1) (2020) 76–87.

[44] L.E. Bertassoni, Progress and challenges in microengineering the dental pulp vascular microenvironment, J. Endod. 46 (9S) (2020) S90–S100.

[45] K. Xia, Z. Chen, J. Chen, H. Xu, Y. Xu, T. Yang, Q. Zhang, RGD- and VEGF-mimetic peptide epitope-functionalized self-assembling peptide hydrogels promote dentin-pulp complex regeneration, Int. J. Nanomed. 15 (2020) 6631–6647.

[46] C.H. Yao, K.Y. Chen, M.H. Cheng, Y.S. Chen, C.H. Huang, Effect of genipin crosslinked chitosan scaffolds containing SDF-1 on wound healing in a rat model, Mater Sci Eng C Mater Biol Appl 109 (2020) 110368.

[47] I. Garzon, M.A. Martin-Piedra, V. Carriel, M. Alaminos, X. Liu, R.N. D'Souza, Bioactive injectable aggregates with nanofibrous microspheres and human dental pulp stem cells: a translational strategy in dental endodontics, J Tissue Eng Regen Med 12 (1) (2018) 204–216.

[48] B. Chang, N. Ahuja, C. Ma, X. Liu, Injectable scaffolds: preparation and application in dental and craniofacial regeneration, Mater. Sci. Eng. R Rep. 111 (2017) 1–26.

[49] Y. Yajima, M. Yamada, R. Utoh, M. Seki, Collagen microparticle-mediated 3d cell organization: a facile route to bottom-up engineering of thick and porous tissues, ACS Biomater. Sci. Eng. 3 (9) (2017) 2144–2154.

[50] M.J. Gupte, W.B. Swanson, J. Hu, X. Jin, H. Ma, Z. Zhang, Z. Liu, K. Feng, G. Feng, G. Xiao, N. Hatch, Y. Mishina, P.X. Ma, Pore size directs bone marrow stromal cell fate and tissue regeneration in nanofibrous macroporous scaffolds by mediating vascularization, Acta Biomater. 82 (2018) 1–11.

[51] S. Jiang, C. Lyu, P. Zhao, W. Li, W. Kong, C. Huang, G.M. Genin, Y. Du, Cryoprotectant enables structural control of porous scaffolds for exploration of cellular mechano-responsiveness in 3D, Nat. Commun. 10 (1) (2019) 3491.

[52] R.K. Kankala, J. Zhao, C.G. Liu, X.J. Song, D.Y. Yang, K. Zhu, S.B. Wang, Y.S. Zhang, A.Z. Chen, Highly porous microcarriers for minimally invasive in situ skeletal muscle cell delivery, Small 15 (25) (2019), e1901397.

[53] S.T. Koshy, D.K.Y. Zhang, J.M. Grolman, A.G. Stafford, D.J. Mooney, Injectable nanocomposite cryogels for versatile protein drug delivery, Acta Biomater. 65 (2018) 36–43.

[54] X. Zhang, J. Li, P. Ye, G. Gao, K. Hubbell, X. Cui, Coculture of mesenchymal stem cells and endothelial cells enhances host tissue integration and epidermis maturation through AKT activation in gelatin methacryloyl hydrogel-based skin model, Acta Biomater. 59 (2017) 317–326.

[55] G. Lei, Y. Yu, Y. Jiang, S. Wang, M. Yan, A.J. Smith, G. Smith, P.R. Cooper, C. Tang, G. Zhang, J. Yu, Differentiation of BMMSCs into odontoblast-like cells induced by natural dentine matrix, Arch. Oral Biol. 58 (7) (2013) 862–870.

[56] L.F. Goncalves, A.P. Fernandes, L. Cosme-Silva, F.A. Colombo, N.S. Martins, T.M. Oliveira, T.H. Araujo, V.T. Sakai, Effect of EDTA on TGF-beta1 released from the dentin matrix and its influence on dental pulp stem cell migration, Braz. Oral Res. 30 (1) (2016) e131.

[57] F.F. Demarco, L. Casagrande, Z. Zhang, Z. Dong, S.B. Tarquinio, B.D. Zeitlin, S. Shi, A.J. Smith, J.E. Nor, Effects of morphogen and scaffold porogen on the differentiation of dental pulp stem cells, J. Endod. 36 (11) (2010) 1805–1811.

[58] A. El-Fiqi, N. Mandakhbayar, S.B. Jo, J.C. Knowles, J.H. Lee, H.W. Kim, Nanotherapeutics for regeneration of degenerated tissue infected by bacteria through the multiple delivery of bioactive ions and growth factor with antibacterial/angiogenic and osteogenic/odontogenic capacity, Bioact Mater 6 (1) (2021) 123–136.

[59] A. Stein, A. Stroobants, V. Gieselmann, R. D'Hooge, U. Matzner, Anti-inflammatory therapy with simvastatin improves neuroinflammation and cns function in a mouse model of metachromatic leukodystrophy, Mol. Ther. 23 (7) (2015) 1160–1168.

[60] A. Hot, F. Lavocat, V. Lenief, P. Miossec, Simvastatin inhibits the pro-inflammatory and pro-thrombotic effects of IL-17 and TNF-alpha on endothelial cells, Ann. Rheum. Dis. 72 (5) (2013) 754–760.

[61] M. Goldberg, A. Njeh, E. Uzunoglu, Is pulp inflammation a prerequisite for pulp healing and regeneration? Mediat. Inflamm. 2015 (2015) 347649.

[62] B. Sui, C. Chen, X. Kou, B. Li, K. Xuan, S. Shi, Y. Jin, Pulp stem cell-mediated functional pulp regeneration, J. Dent. Res. 98 (1) (2019) 27–35.

[63] M. Torabinejad, R. Corr, M. Buhrley, K. Wright, S. Shabahang, An animal model to study regenerative endodontics, J. Endod. 37 (2) (2011) 197–202.

[64] S.N. Kaushik, B. Kim, A.M. Walma, S.C. Choi, H. Wu, J.J. Mao, H.W. Jun, K. Cheon, Biomimetic microenvironments for regenerative endodontics, Biomater. Res. 20 (2016) 14.